Sediment thickness in the Thrace Basin estimated from the three-dimensional inversion of magnetotelluric data

Cemal Kaya[a] and Ahmet Tuğrul Başokur[b]

[a] *(deceased)General Directorate of Mineral Research and Exploration, Department of Geophysics, Ankara, Türkiye. Orcid ID 0000-0002-2683-1043.*

[b] *Lemnis Yerbilimleri, Ankara Üniversitesi Teknokent, 06830 Gölbaşı, Ankara, Türkiye. Orcid ID 0000-0002-5981-8937.*

**Corresponding author: Ahmet Tuğrul Başokur, basokur@ankara.edu.tr*

In Memoriam

by Ahmet Tuğrul Başokur

The first author, Cemal Kaya, passed away in February, 2022. The Turkish geophysical community will always remember Cemal Kaya's friendship, honesty and sincerity. He graduated from Istanbul Technical University (ITU) Faculty of Mines, Department of Geophysical Engineering in 1981. He started his career as a geophysical engineer at the General Directorate of Mineral Research and Exploration. He completed his MS and PhD under my supervision at Ankara University. We completed many research projects in the 1990s, including the controlled-source audio-magnetotelluric (CSAMT) method for massive sulfide exploration and the magnetotelluric method in geothermal resource exploration, the first examples in Türkiye. We also initiated the systematic use of the MT method in crustal research as a joint TÜBITAK project of Ankara University and the General Directorate of Mineral Research and Exploration in 1995. This article is the first profile of national crustal research project. Since only two-dimensional modelling could be applied in the 1990s, a conductive artefact zone appeared under the Hisarlıdağ uplift in the resistivity model since the Thrace Basin surrounded by the Aegean, Marmara and Black Seas on three sides. Now, we have constructed a more realistic model of the Thrace Basin using the three-dimensional modelling that permits including the seabed topography.

ABSTRACT

The time-variation of the magnetotelluric (MT) fields was recorded at 37 measurement stations in the Thrace Basin (North-western Türkiye) by a remote-reference MT system that records the MT data in two frequency bands allowing a data acquisition between 320–7.5 Hz and 6–0.00055 Hz, respectively. The measurement stations were

located from the Aegean Sea to the Black Sea seashores along a 207 km profile in the southeast-northwest direction. Three-dimensional inversion of MT data outlined the main geological elements of the region, the interface between sedimentary cover and basement rocks. The total thickness of the sedimentary layers in the basin is interpreted using the inflection and deflection points of the three-dimensional resistivity model in the vertical direction.

Key Words: Three-Dimensional Magnetotelluric Inversion, Thrace Basin, Sediments Thicknesses.

1. Introduction

MT studies have been used to investigate oil, gas and geothermal reservoirs, deep sedimentary basins, the upper mantle and the crustal thickness for more than six decades (Swift, 1967; Vozoff, 1972; Jupp and Vozoff, 1977; Beblo et al., 1983; Wannamaker, 1983; Hersir and Björnssonn, 1991; Lezaeta et al., 2000; Gokarn et al., 2008; Kaya, 2010; Hacıoğlu et al., 2020; Başokur et al., 2022; Hacıoğlu et al., 2023). We used the MT method to investigate the thickness of the sedimentary layer in the Thrace Basin of northwestern Türkiye because of its cost-effective implementation along a profile. The basin is one of the most important hydrocarbon production areas in Türkiye (mainly natural gas). The existing drill holes ended in the sedimentary cover around the MT line. An estimation for the total sediment thickness was published by Siyako and Huvaz (2007) using seismic and well data as a contour map. Three-dimensional inversion of MT data provides additional information about the shape and depth of the basement along the 207 km line between the Aegean and Black Seas seashores.

2. Geology of the Thrace Basin

The Thrace Basin is considered to be an intramontane Tertiary basin surrounded by the Strandja in the north, the Rhodope in the west, the Istanbul Zone in the east, and the Sakarya Continent and Intra-Pontid Suture in the south, as shown in Figure 1. The basement of the surrounding massifs consists of metamorphics, Istanbul Paleozoic-Mesozoic sedimentary sequences, ophiolitic melanges and occasional igneous bodies of the pre-Upper Cretaceous age (Turgut et al., 1983; Doust and Arıkan, 1974; Siyako and Huvaz, 2007). Okay et al.(2023) partitioned the sedimentary layers into three sequences separated by major unconformities: Lower-middle Eocene, Middle/upper Eocene—Oligocene, and Miocene-Pliocene. The basin is elliptical, and its long axis extends in the southwest-northeast direction. A series of basement step faults limits the basin in NE, and a fault scarp controls the flanks of the basin in SE. Very thick flysch-type clastics were due to a very fast subsidence. Some clastic materials were deposited in the Lower Oligocene because of continuous transgression that caused the

submergingof the southwestern parts of the basin. In contrast, the carbonates were deposited on the northern shelf simultaneously. An active volcanism caused dacitic and andesitic ashes. In the Middle Oligocene, the subsidence slowed, and the basin's depositional environment became lacustrine and fluviatile. The deposition continued without interruption until the Upper Oligocene. Volcanic activities lost intensity in the Upper Oligocene (Turgut et al., 1983; Siyako, 2006).

Doust and Arıkan (1974) postulated that a major erosional phase caused the removal of much of the Lower and Upper Oligocene sediments into the centre and southern part of the basin. The Lower and Upper Oligocene sedimentary sequence demonstrates a transgressive-regressive depositional cycle that includes shallow marine sediments. A major tectonic event in the Middle Eocene gave rise to faulting and folding in the SW-NE direction. The late Pliocene tectonic activities shaped the present configurations of the basin (Turgut et al., 1983). On the other hand, according to Perinçek (1991) and Perinçek et al. (2015*a*), the final most important tectonic event in Thrace Basin occurred before the deposition of Ergene formation. Thrace fault system became active before the Ergene formation and continued during the sedimentation of it. Thrace fault systems cause uplift and erosion along the fault zones (Perinçek et al., 2015*b*).

Two tectonic trends are dominant in the study area. 1) The Ganos Mount trend is in the NE-SW direction parallel to the Ganos Mount and constitutes the southward limit of the basin. 2) The Strandja trend has an NW-SE strike parallel to the Strandja basement ridge, limiting the north basin (Doust and Arıkan 1974). Coşkun(1997) postulates that the older structures trending in the NE-SW direction were influenced by basement paleotopography, and the younger structures trending in the NW-SE direction were under the influence of the North Anatolian Fault (NAF). Perinçek(1991) interpret the Thrace fault system as the oldest strand of the North Anatolian Fault, releasing-bend extensional structures. The Thrace strike-slip fault system consists of the west-northwest-striking Kirklareli, Lüleburgaz, and Babaeski fault zones that are inactive presently (Perinçek, 1991).

The collision between the Sakarya and Rhodope continents leads to lateral movements and normal basement faults, which become detachment faults during the subsequent opening of the Thrace Basin (Turgut et al., 1991; Tüysüz et al., 1998). The Bouguer gravity map clearly shows these trends and, the thick basin fills are represented by a low value of gravity anomalies (Figure 2). Sakınç et al. (1999) suggested that the basin principally developed by the activities of the Thrace and Ganos strike-slip fault systems following the continental collision during the Late Oligocene-Early Miocene period. Thrace Basin was opened during the Middle Eocene on Strandja Massif as a post-collisional fault-controlled extensional basin and turned into an intramontane basin in the Middle Miocene (Tüysüz et al. 1998). However, a fore-arc origin for the Thrace Basin has been proposed, which is linked to the

subduction of the Intra-Pontide Ocean between the Middle Eocene and Oligocene. The Rodope-Pontide magmatic arc was developed on the overriding Strandja zone and started to rift and extend, forming the Thrace Basin (Görür and Okay, 1996).

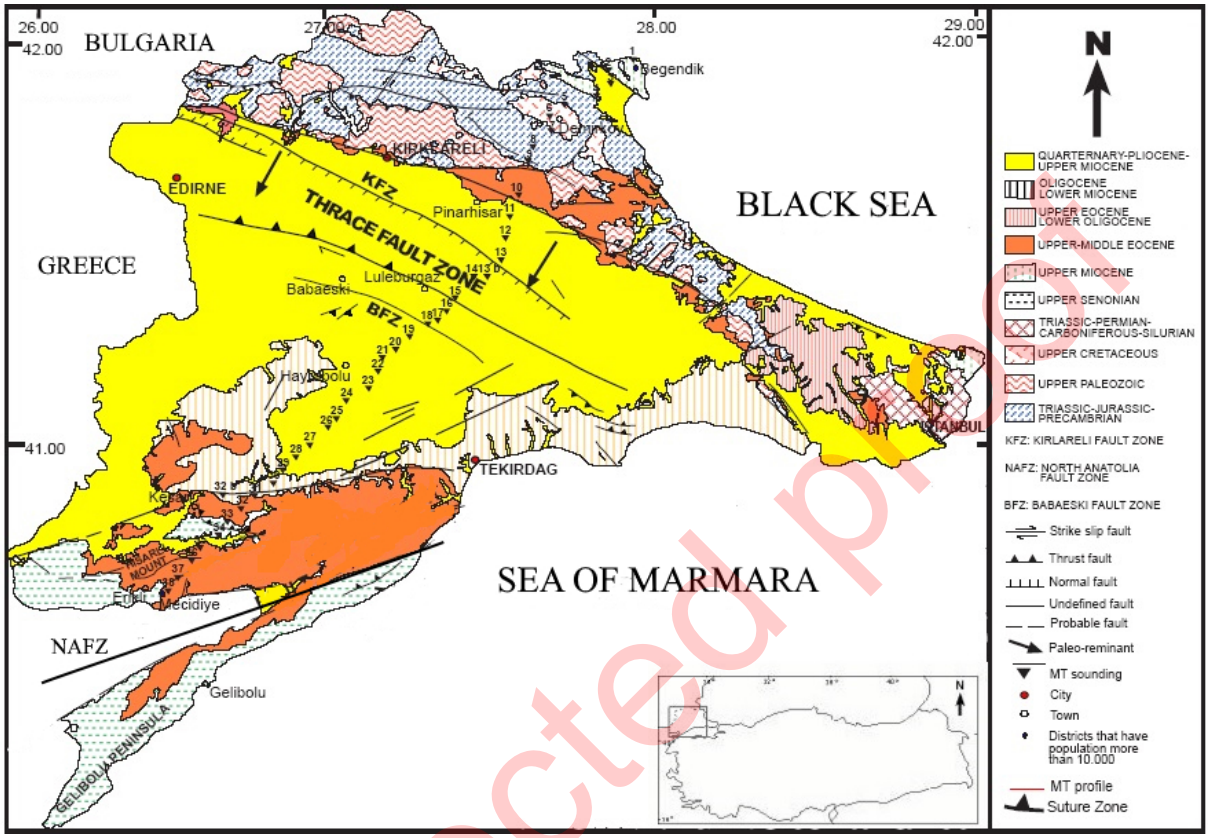

Figure 1- Geological map of Thrace Basin and MT stations (station numbers over triangles), modified from the Geological Map of Türkiye, General Directorate of Mineral Research and Exploration.

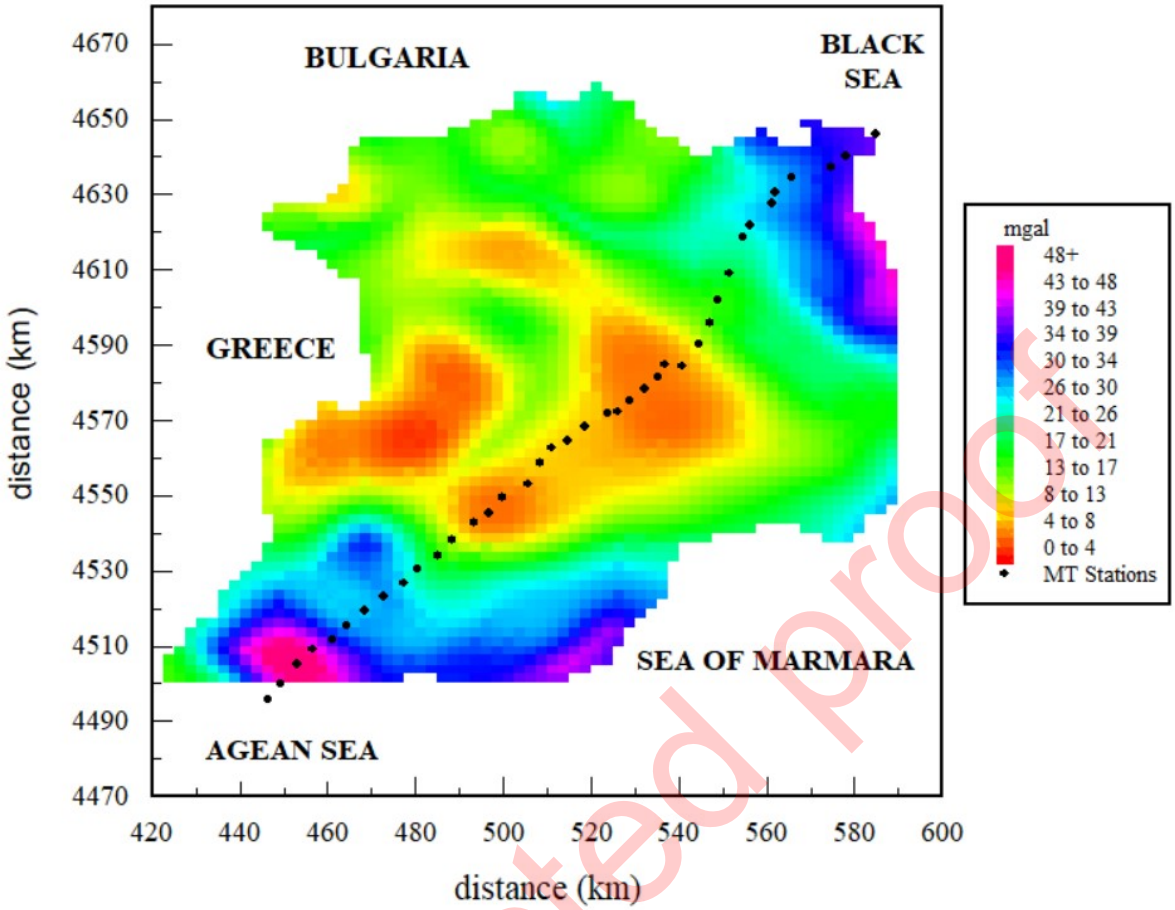

Figure 2- Location of MT stations used in this study over Bouger gravity anomaly map (MTA, 1999).

3. Data Acquisition and Processing

The MT profile lies in the southwest-northeastern direction from the Aegean Sea to the Black Sea and consists of 40 measurement stations (Figure 1). Station intervals ranged from 4 to 5 km, depending on the accessibility of the territory. The total length of the profile was 207 km. The first and last measurement stations were close to the Black Sea and Aegean coast.

The magnetotelluric (MT) method simultaneously measures orthogonal components of the natural horizontal electric and magnetic fields. The electromagnetic variations, lasting longer than 1 second, consist of micropulsations originating from the earth's magnetosphere's interaction with charged particles ejected from the sun and other sources. Lightning strokes almost entirely generate electromagnetic variations below one second. Phoenix-V5 equipment was used to acquire MT data consisting of three orthogonal magnetic (*H*) and two orthogonal electric (*E*) field components. MT electrical dipoles of 100 m, equal to the length of one side of the TEM transmitter loop, were applied to measure E-fields in NS and EW directions. Nonpolarizable lead-lead chloride (Pb-$PbCl_2$) electrodes were used for E-field measurement because of their long-term stability of

polarization (Petiau and Dupis, 1980). Induction coils and an air loop on the ground were used to measure the horizontal and vertical components of the magnetic fields, respectively. Additional two orthogonal magnetic fields were measured at a remote reference station.

The data were acquired in two steps by measuring high and low frequency bands in 1995. The high band consisted of 12 frequencies between 320 and 7.5 Hz. There were 28 frequencies in the low band in the range of 6-5.493x10^{-4} Hz. MT records were acquired for more than 24 hours in the lower band. The impedance values in 40 frequencies were combined in the frequency domain after the Fourier transformation of time-domain data using cascade decimation (Wight and Bostick, 1980).

The orthogonal components of the horizontal electric and magnetic fields measured in the time-domain are linearly dependent. Consequently, their Fourier transform leads to a 2x2 tensor, and its elements are called impedances (*Z*). Impedance values are estimated from a complex electric field (E) ratio over the magnetic field (*H*) in the frequency domain. The tipper (*T*) connects the vertical and two horizontal magnetic fields. The impedance tensor and tipper vector are given in the frequency domain after the application of Fourier transformation as follows:

$$\begin{pmatrix} E_x \\ E_y \end{pmatrix} = \begin{pmatrix} Z_{xx} & Z_{xy} \\ Z_{yx} & Z_{yy} \end{pmatrix} \begin{pmatrix} H_x \\ H_y \end{pmatrix},$$

$$\begin{pmatrix} H_z \end{pmatrix} = \begin{pmatrix} T_x & T_y \end{pmatrix} \begin{pmatrix} H_x \\ H_y \end{pmatrix}$$

where *x* and *y* denote the orthogonal components in the north and east directions, and *z* indicates the vertical component. The impedances are always a decreasing function of the period, and the shape of MT curves is independent of subsurface resistivity distribution. Then, the general behaviour of impedance data may not give any idea about the resistivity variation in the subsurface. The following normalization improves the physical significance of the data (Başokur, 1994; 1999):

$$F = \frac{Z}{\sqrt{i\omega\mu}} = \frac{1}{\sqrt{i\omega\mu}} \frac{E_x}{H_y}$$

where $i = \sqrt{-1}$. *F* is named as the frequency normalized impedance or shortly FNI. The unit of the FNI function is the square root of ohm-m ($\sqrt{ohm-m}$). μ and ω denotes the magnetic permeability of free space and angular

frequency, respectively. This normalization connects the measured data and the subsurface resistivity distribution and directly reflects resistivity variations versus depth as the function period (Başokur, 1999; Başokur, 2023). The validity of the measured MT data can be tested using the causality concept. Başokur (2023) proved that the real and imaginary parts of the FNI function can be calculated from each other via the Hilbert transform. This procedure help check if the data satisfies natural EM field conditions. As an example, Figure 3 shows the measured and Hilbert-transformed FNI data for the station 33 and proves the data validity for this station.

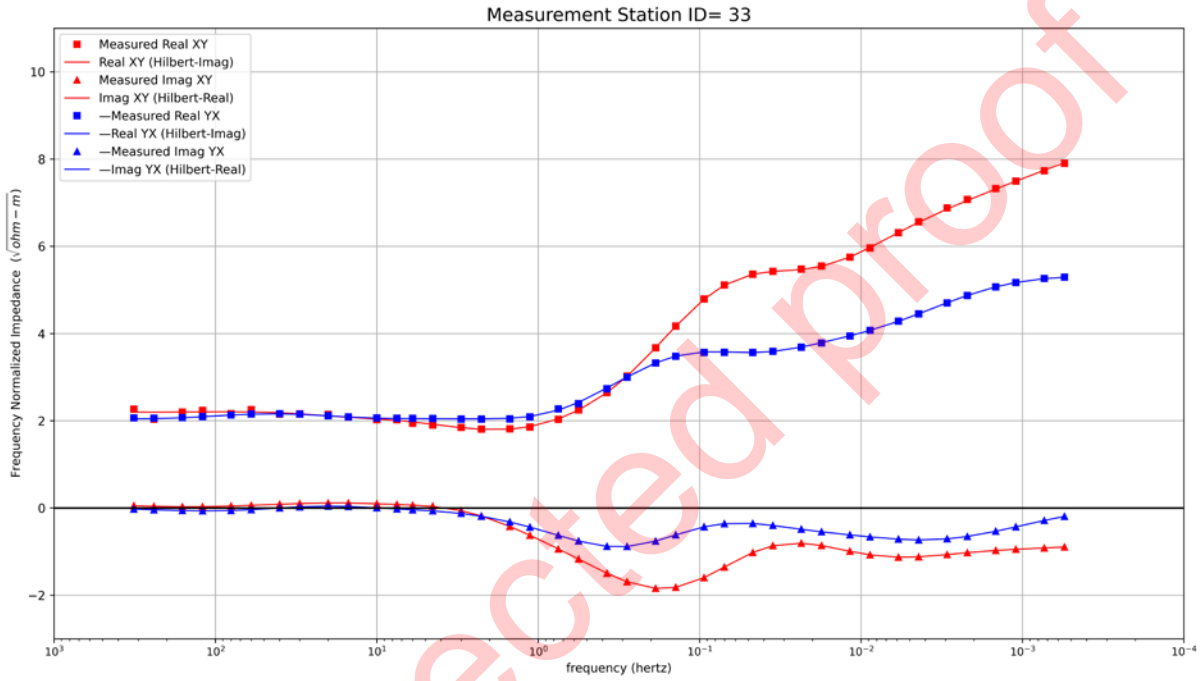

Figure 3- Frequency normalized impedance, real (squares) and imaginary (triangles) components, and their corresponding Hilbert transforms (continuous curves).

4. Three-dimensional Inversion

The purpose of geoelectrical data inversion is to estimate the subsurface resistivity distribution. A resistivity model is derived indirectly by searching for a fit between theoretical data computed for a conceptual model and the measured data. The most commonly used conceptual models are 1D, 2D or 3D subsurfaces in historical order. The reliability of the derived model is dependent on the consistency of the conceptual model with the actual surface conditions. The type of conceptual model should be decided before geophysical exploration so that the survey design can be planned according to the selected conceptual model. All constants defining a particular conceptual model are named 'model parameters'. A 3-D model consisting of a huge number of cube-shaped cells is preferred for a better description of subsurface physical conditions. Usually, the inversion algorithm is initialized by a homogeneous earth model by assigning the same resistivity value to all model cells. The model

parameters only comprise the resistivity values of each cell. Keeping the geometry of cells constant during iterations drastically reduces the number of model parameters to be estimated. Then, the cell resistivity values are updated iteratively by computing a parameter update vector at each iteration from the differences between measured and theoretical data sets (Başokur and Akca, 2011). Models corresponding to misfit values *E(p)* lower than a threshold are considered a possible solution to represent subsurface resistivity distribution. The reduction of misfits along successive iterations is not sufficient to obtain a smooth and geologically acceptable model. Also, preventing random resistivity changes among neighbouring cells is necessary. For this purpose, a stabilizer function *S(p)* is added in the objective function $\phi(p)$ to control the model resistivity variations as follows:

$$\phi(p) = E(p) + \alpha S(p)$$

where α is the regularization coefficient. The misfit function is defined as the sum of the square of the differences between measured and calculated data values at each frequency:

$$E(p) = \sum_{i=1}^{n} \frac{(d_i - f_i)^2}{\sigma_i^2} .$$

d_i and f_i are the measured and theoretical data, respectively. σ_i is the standard deviation corresponding to *ith* frequency value. *n* is the number of measured data values. The *nmrs* value quantifies the degree of misfit, and an *nmrs* value which is lower than three is expected in the final step of inversion:

$$nrms = \frac{1}{n}\left[\sum_{i=1}^{n} \frac{(d_i - f_i)^2}{\sigma_i^2}\right]^{1/2} .$$

We used the 3D non-linear conjugate gradient (NLCG) software named ModEM (Egbert and Kelbert, 2012; Kelbert et al., 2014). ModEM is a modular system of parallel computer codes for the inversion of electromagnetic (EM) geophysical data and uses the following stabilizer function:

$$S(p) = \sum_{j=1}^{m} \frac{(m_j - m_j^0)^2}{\sigma_j^2}$$

where m_j is the resistivity value of *jth* cell and m_j^0 corresponds to the initial resistivity value of a priory model. σ_j represents the model covariance value corresponding to the *jth* cell. *m* is the number of model parameters. A 3-D MT inversion requires a lot of computing time despite using a multi-core cluster and parallelized calculations. The computation was performed using an HP ProLiant DL580 Gen10 computer with 80 cores.

Bayrak et al. (2006) applied a dimensional analysis to the current MT data. They concluded that the high-frequency part, corresponding to the younger sedimentary fills, shows a 1D behaviour, while the data at the low frequencies show a 3D behaviour. Consequently, we applied 3D inversion and the bathymetry of the Black Sea, Marmara and Aegean Seas were inserted into the model and a sea resistivity value of 0.33 ohm-m was assigned to represent their contribution to the data. The total number of cells is equal to 646,000. The topography is modelled from SRTM90 data. An average elevation is used for the *z* coordinate of the top of the corresponding cell. Figure 4 shows the 3D modelling grid in the x-y plane comprising 85 and 80 cells, respectively. The model is also extended to 95 cells in the z-direction. The total number of parameters to be solved is 646.000. The ModEM software has been executed in a cluster so that one processor serves the calculation of the theoretical data for one frequency. The inverted data consists of 40 sample values in the range of frequencies between 320 and and 5.493×10^{-4} Hz.

The Thrace Basin consists of a sediment layer with low resistivity, so the industrial noise was attenuated relatively short distances. Because of its higher resistivity values, the noise contribution over Strandja Massif was higher than that of the basin in intermediate and long periods. The two off-diagonal components of the impedance tensor have been used in the inversion. However, the diagonal components corresponding to the low frequencies were scattered while almost zero at the high-frequency band because of the thick 1D sedimentary cover. For these reasons, the diagonal components were not used in the inversion. The tipper values have been disregarded because of high noise contamination. The algorithm was initialized with homogeneous resistivity values of 100 ohm-m. Meanwhile, various error levels and smoothing factors for horizontal and vertical directions were used for each initial-guess model. Finally, the model produced the smallest misfit (*nrms*) value of 1.8 after 55 NLCG iterations. The measured and calculated curves corresponding to station 33 are shown in Figure 5.

Figure 6 shows the FNI pseudo-sections of the measured and calculated data in a distance-frequency (*x*-*f*) plane for the *YX* component. It can be concluded that the final 3D model produced a satisfactory fit between the measured data and model response, and there are no artefacts in the model due to noise or surrounding seas. The pseudo-

section derived from the measured data indicates the shape of the basement since the MT profile is almost perpendicular to the geological strike of the basin.

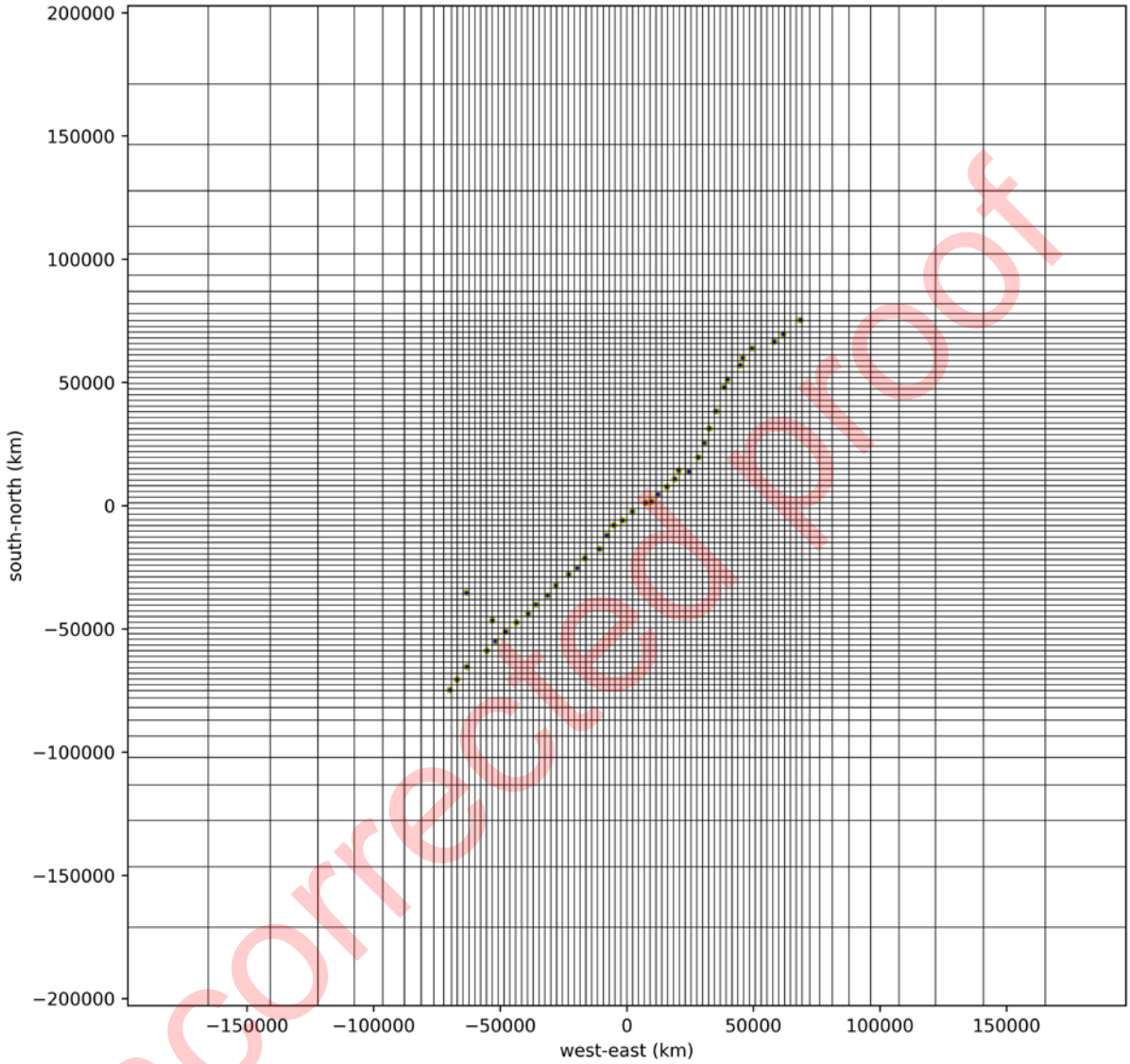

Figure 4- Plan view (x-y plane) of the modelling grid used in the 3-D inversion. The yellow dots show measurement stations. The survey area is subdivided into 646,000 cells. There are 85, 80 and 95 cells in the north, east and depth.

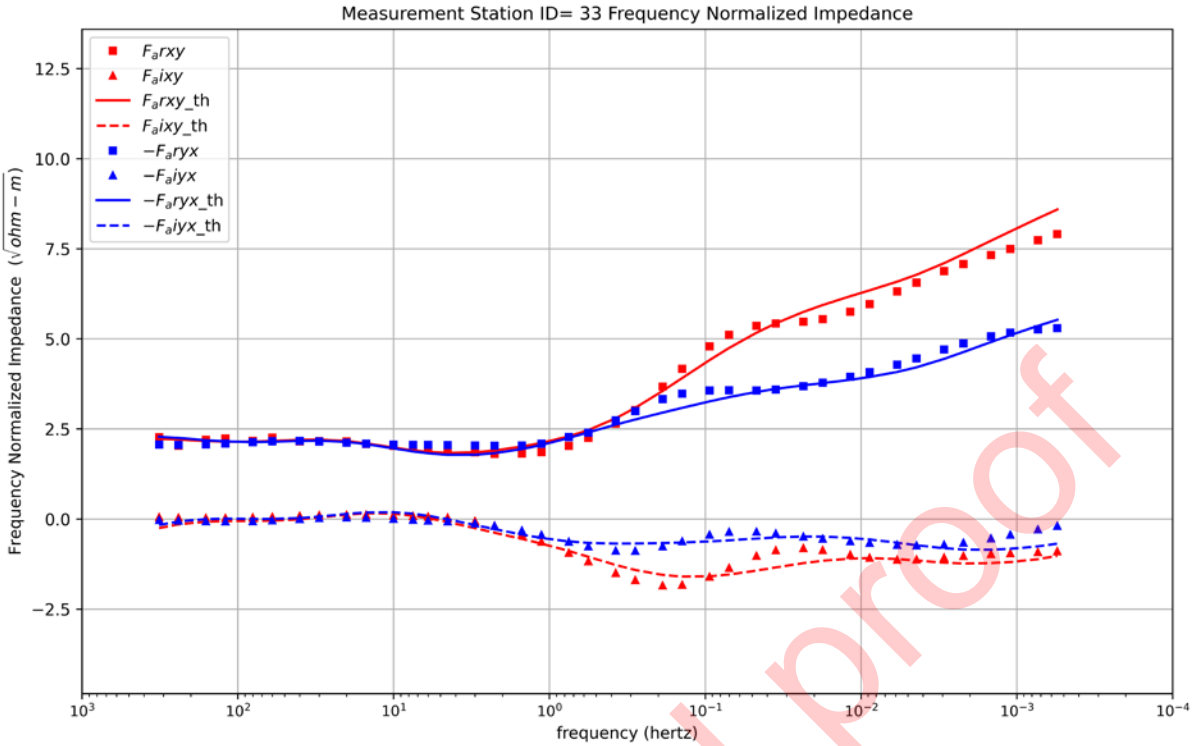

Figure 5-Data fit for the 3D inversion at station 33. The red and blue colours indicate the xy and yx components. Squares and triangles show the measured real and imaginary components, respectively. The continuous curves are the model responses.

5. Interpretation

Figure 7a illustrates the final model obtained from the 3D inversion. A cell was colourized by a specific colour proportional to its intrinsic resistivity value. The resistivity limits were selected in the range [0,3] log10 ohm-m corresponding to the resistivity values of 1 and 1000 ohm-m in a linear scale, respectively. The selected resistivity scale better reflects the shape of the basin due to the high resistivity contrast between relatively low resistivity young sediments and high resistivity basement. However, interpreting the depth of interfaces using a colour scale will remain subjective. Changing the resistivity scale of the colour map will produce images in which the probable location of interfaces will be perceived differently. This is the main difficulty in identifying the layer interfaces by visual inspection. Akca and Başokur(2010) developed the concept of the structure-based model in which the model parameters simulate undulating interfaces in 2D subsurface. However, the conventional derivative-based inversion methods could not be applied to the structure-based model parameterization. Searching for a model that produces minimum misfit can be performed by model verification algorithms that generate and verify many distinct and complicated models. For cases where many models should be verified, the genetic algorithm is one of the most

suitable for verifying large model sets (Başokur et al., 2007). However, the computation of 3D models is expensive and time-consuming, so the next computer generation can tackle constructing structure-based 3D models.

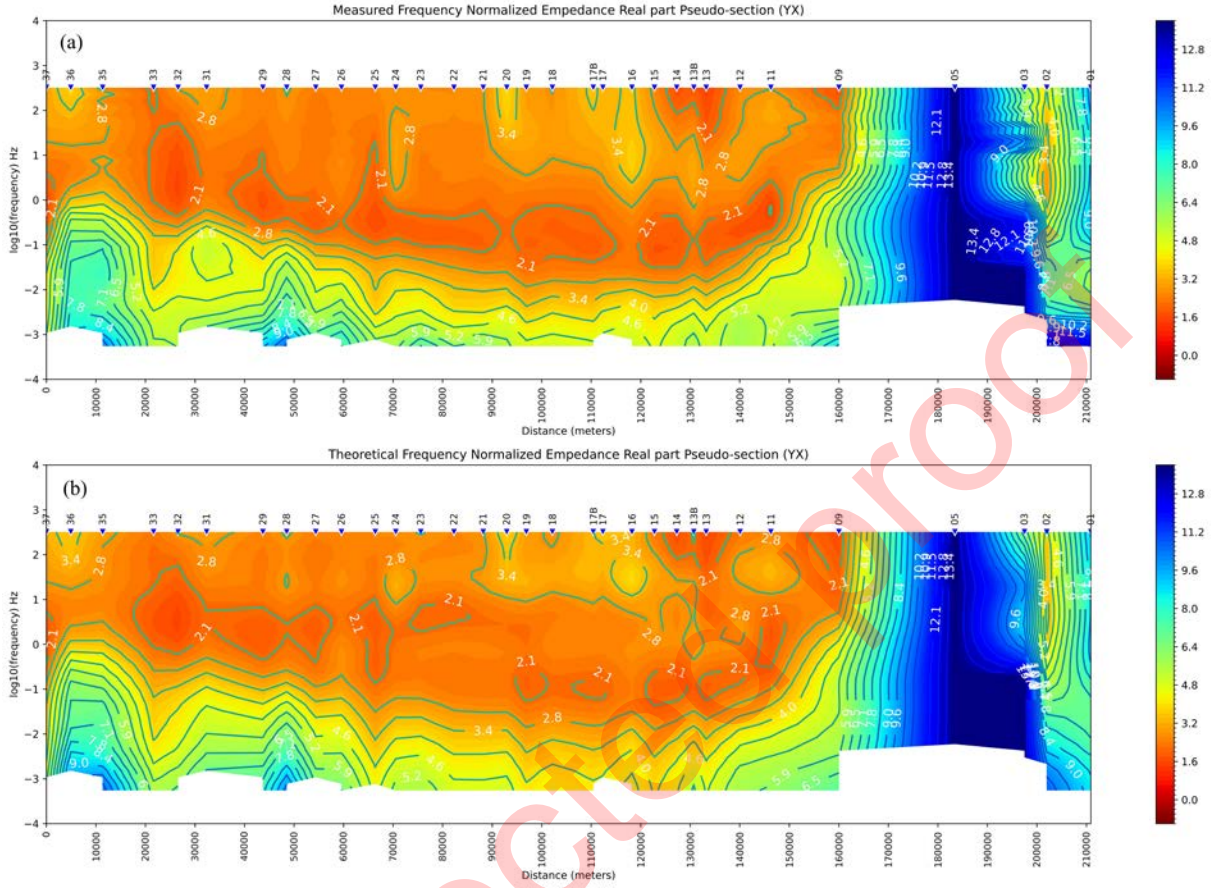

Figure 6- Comparison of the measured (a) and calculated (b) real parts of the FNI function for the YX component pseudo-sections.

ModEM software produces smooth models; consequently, the resistivity versus depth is a smooth curve. For this reason, we apply the scheme developed by Başokur(2022) to delineate possible interfaces. The variation of resistivity along a column in the vertical direction with the same central x and y coordinates is extracted as a function of *z* values from the smooth model. For example, Figure 8 shows the depth-resistivity curve derived from the 3D model cube for particular x-y coordinates corresponding to station 23 (black lines). The maxima, minima, (magenta dots in Figure 8) inflection and deflection points (red dots) can be derived using the NymPy library of Python (https://numpy.org/) from the first and second numerical derivatives, respectively. The inflection and deflection points of the depth-resistivity (*z-rho*) curve are the most probable boundaries of the interfaces since they

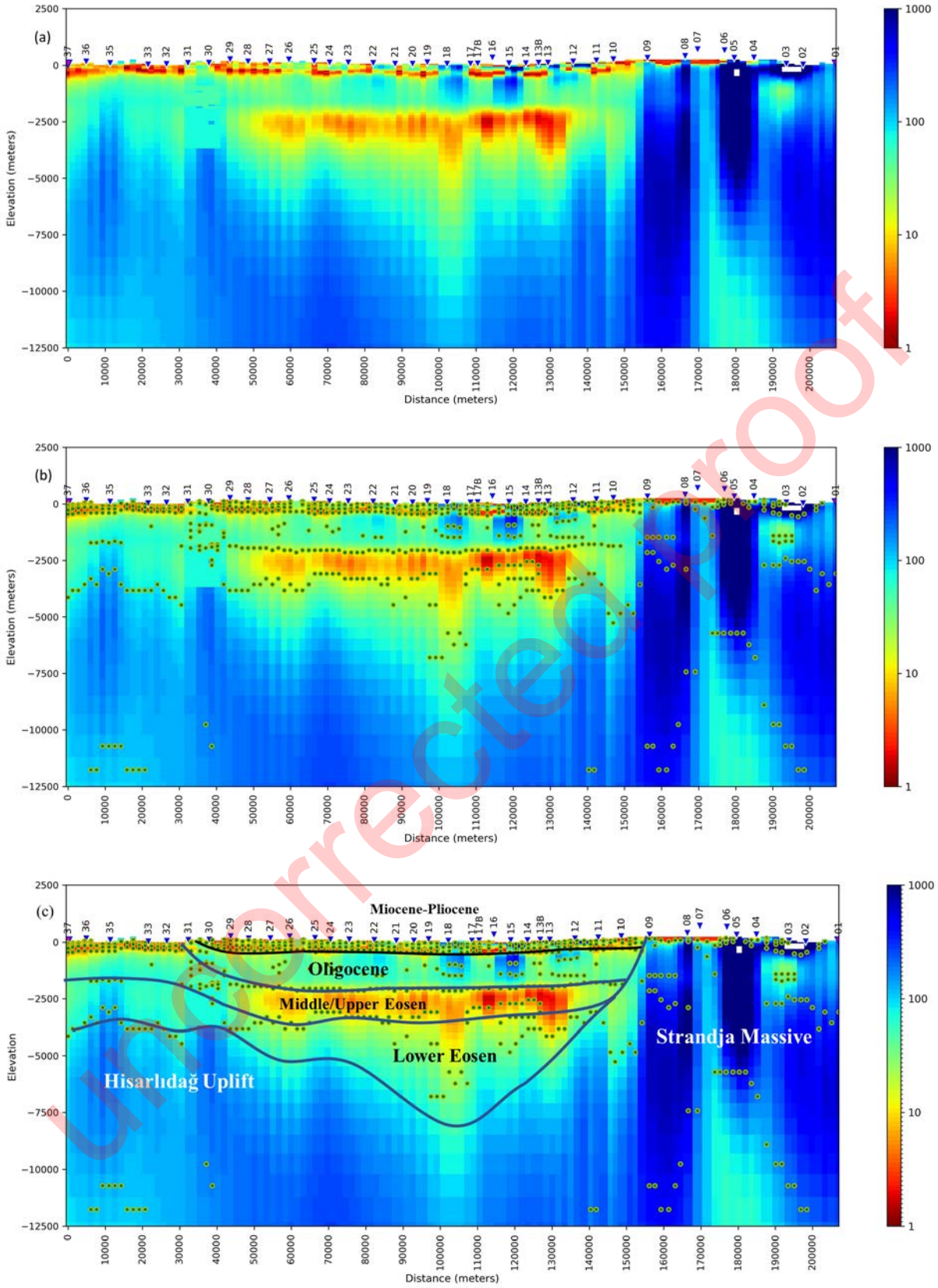

Figure 7- Resistivity section derived from the 3D inversion (a). The inflection and deflection points of the model in the vertical direction (b). Possible interpreted interfaces (c).

indicate sharp resistivity variations. The applied procedure is similar to edge detection algorithms. A subsurface model is constructed by connecting the points (green lines in Figure 8). The method can be repeated for all *z-rho* curves along a profile, and possible layer interfaces can be plotted as dots over a resistivity section (Figure 7b). This numerical strategy helps the interpreter identify the layer interfaces from a cell-based smooth 3D model.

Figure 7c illustrates our interpreted model derived from the dotted inflection and deflection points. There is no significant sedimentary cover on the top of the Strandja massif. The slope variations in the basement floor were well delineated because of the high resistivity contrast between sedimentary units and crystalline basement. The overall interpretation could imply that major structural elements of the region could be outlined with the help of the MT method without much difficulty. Moreover, the main fault zones may be identified with the help of the information obtained from the surface geology. The depth to the basement along the MT profile reaches 8000-8500 meters. However, the total sediment thickness can reach 10-11 km at the east of the MT profile. A depth estimate using the power spectrum of the gravity data produces a similar result.

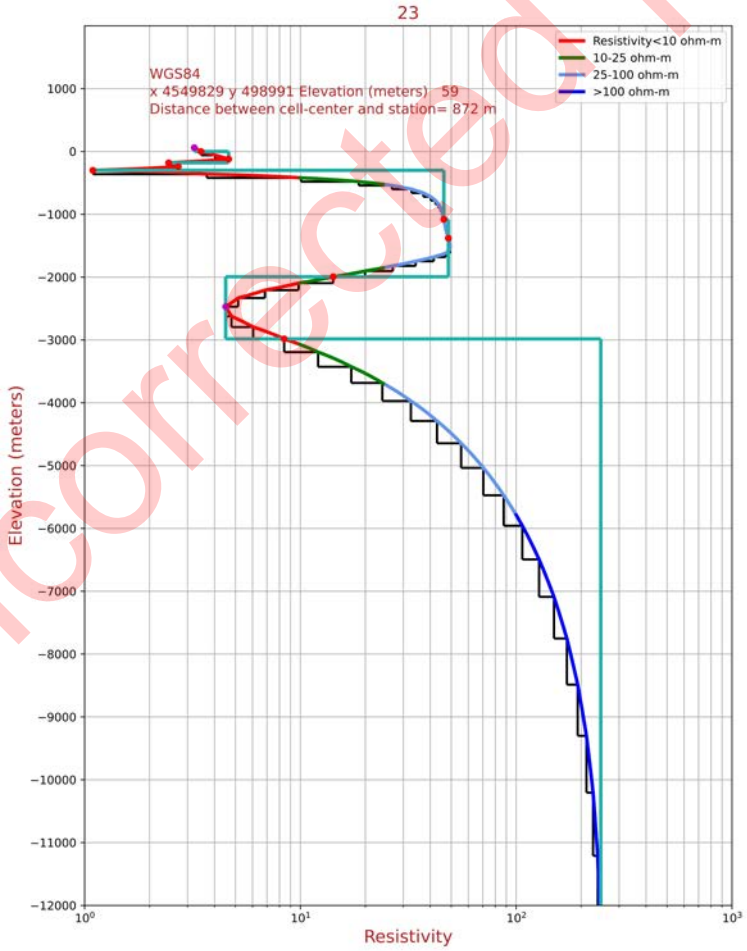

Figure 8- Resistivity variation with depth. Black lines are the resistivity values of each cell. Blue lines indicate the probable depth of interfaces.

6. Discussion and Conclusion

There have been three different suggestions for the location of the Intra-Pontid suture zone representing the boundaries of former Sakarya and Rhodope continents: (1) It has been suggested that a suture of the Intra-Pontide Ocean existed between Strandja Massif and Sakarya continent as noted by Şengör and Yılmaz(1981). The ocean closed during the Cretaceous to Palaeocene period. However, there has been a controversy over the existence and location of this suture zone. It has been proposed that the suture was located at the south of the Thrace Basin, extending towards the west-east direction along the north coast of the Aegean Sea towards the Marmara Sea, as reported by Şengör and Yılmaz(1981). (2) The north of the Strandja massif has been suggested to be the location of the suture zone (Yılmaz *et al*. 1997). (3) Bayrak et al. (2004) reported that the suture was an N-S-oriented zone between İstanbul and Çatalca in the north. They have also proposed an alternative location close to the surface contact between Thrace Basin and the Strandja massive in the north based on the interpretation of their nine magnetotelluric stations. Their short profile extended approximately in the N-S direction from Strandja Massif towards the Sea of Marmara. It crossed our MT line around station 13 and contained no information about the south of station 13. A possible location may correspond to the low resistivity anomaly beneath stations 12 and 13 in Figure 7c. Additional MT profiles parallel to the existing line are required to resolve the exact location. Modelling over an MT profile data with distant stations would not allow a detailed geological interpretation. Still, we demonstrate that the MT method could map sedimentary cover and undulations in the basement. Also, the present study shows that the main differences in the depth of the conductive units of Thrace and other similar sedimentary basins can be inexpensively delineated over large areas using the MT method.

ACKNOWLEDGEMENTS

This paper is part of the National Geology and Geophysics Programme (Naci Görür, coordinator) supported by TUBİTAK, Project No. YDABÇAG-230/G. The MT data was acquired in the framework of the Turkey Earth Crust Project (TECP) performed by the General Directorate of Mineral Research and Exploration of Turkey (MTA) in 1995. I thank Muzaffer Siyako and Doğan Perinçek for critically reading the manuscript and for their suggestions and corrections. M. Siyako also helped with the interpretation shown in Figure 7c.

References

Akca, İ. and Başokur, A. T. 2010. Extraction of structure-based geoelectric models by hybrid genetic algorithms. Geophysics 75, F15-F22.

Başokur, A. T. 1994. Definitions of apparent resistivity for the presentation of magnetotelluric sounding data. Geophysical Prospecting 42, 141-149.

Başokur, A. T. 1999. Properties of the magnetotelluric frequency-normalized impedance function over a layered medium. Journal of the Balkan Geophysical Society 2, 63-74.

Başokur, A. T. and Akca, İ. 2011, Object-based model verification by a genetic algorithm approach: application to archaeological targets, Journal of Applied Geophysics, 74, 167–174.

Başokur, A. T. 2022. Open-source Python software for the visualization of magnetotelluric data and three-dimensional resistivity models. 25th EM Induction Workshop, 11–18 September 2022, Çeşme, Türkiye.

Başokur, A. T. 2023. Hilbert transform of unequally sampled data: Application to dispersion relations in magnetotellurics. Geophysics 88(2), E29-E38.

Başokur, A. T., Akca, İ., Siyam, N. W. A. 2007. Hybrid genetic algorithms in view of the evolution theories with application for the electrical sounding method. Geophysical Prospecting 55, 393–406.

Başokur, A. T., Koçyiğit, A., Hacıoğlu, Ö, Arslan, H. İ., Meqbel, N. 2022. Magnetotelluric imaging of the shallow-seated magma reservoir beneath the Karadağ stratovolcano, Central Anatolia, Turkey. Journal of Volcanology and Geothermal Research 427, 107567.

Bayrak, M., Gürer, A., Gürer, Ö. F. 2004. Electromagnetic imaging of the Thrace Basin and Intra-Pontide subduction zone, Northwestern Turkey. International Geology Review 46, 64-74.

Bayrak, M., Gürer, A., Gürer, Ö. F., İlkisik, M., Başokur, A. T. 2006, Mohr-circle-based rotational invariants of a magnetotelluric data set from the Thrace region of Turkey: Geological implications. Turkish Journal of Earth Sciences 15, 95-110.

Beblo M., Bjornsson A., Arnason K., Stein B., Wolfgram P. 1983. Electrical-conductivity beneath Iceland – constraints imposed by magnetotelluric results on temperature, partial melt, crust-structure and mantle structure. Journal of Geophysics 53**,** 16-23.

Coşkun, B. 1997. Oil and gas fields-transfer zone relationships, Thrace Basin, NW Turkey. Marine and Petroluem Geology 14**,** 401-416.

Doust, H., Arıkan, Y. 1974. The geology of the Thrace Basin. Proceedings of Second Petroleum Congress of Turkey, 119-136.

Egbert, G. D., Kelbert, A. 2012. Computational recipes for electromagnetic inverse problems. Geophysical Journal International 189, 167–251.

Gokarn, S.G., Gupta, G., Walia, D., Sanabam, S. S., Hazarika, N. 2008. Deep geoelectric structure over the Lower Brahmaputra valley and Shillong Plateau, NE India using magnetotellurics. Geophysical Journal International 173, 92–104.

Görür, N., Okay, A. I. 1996. A fore-arc origin for the Thrace Basin, NW Turkey. Geologische Rundschau 85, 662-668.

Hacıoğlu, Ö, Başokur, A. T., Meqbel, N., Arslan, H. İ., Efeçınar, E. 2023. Magnetotellurics unveils a hidden caldera complex beneath the Cappadocia Volcanic Province, Central Anatolia, Turkiye. Journal of Volcanology and Geothermal Research 442, 107877.

Hacıoğlu, Ö, Başokur, A. T., Diner, Ç., Meqbel, N., Arslan, H. İ., Oğuz, K. 2020. The effect of active extensional tectonics on the structural controls and heat transport mechanism in the Menderes Massif geothermal province: Inferred from three-dimensional electrical resistivity structure of the Kurşunlu geothermal field (Gediz Graben, western Anatolia). Geothermics 85, 101708.

Hersir, G. P., Björnssonn, A. 1991. Geophysical exploration for geothermal resources principles and application. National Energy Authority, Geothermal Division, Iceland.

Jupp, D. L. B., Vozoff, K. 1977. Resolving anisotropy in layered media by joint inversion. Geophysical Prospecting 25, 460-470.

Kaya, C. 2010. Deep crustal structure of northwestern part of Turkey. Tectonophysics 489, 227–239.

Kelbert, A., Meqbel, N., Egbert, G. D. Tandon, K. 2014. ModEM: A modular system for inversion of electromagnetic geophysical data, Computers & Geosciences 66, 40–53.

Lezaeta, P., Munoz, M., Brasse, H. 2000. Magnetotelluric image of the crust and upper mantle in the backarc of the Northwestern Argentinean Andes. Geophysical Journal International 142, 841-854.

MTA. 1999. Bouger Anomaly Map of Turkey, 1/ 2.000.000 scale. General Directorate of Mineral Research and Exploration (MTA) Publications.

Okay, A. I., Özcan, E., Siyako, M., Bürkan, K. A., Kylander-Clark, A. R. C., Bidgood, M. D., Shaw, D., Simmons, M. D. 2023. Thrace basin—An Oligocene clastic basin formed during the exhumation of the Rhodope Complex. Tectonics 42, e2023TC007766.

Perinçek, D. 1991. Possible strand of the North Anatolian Fault in the Thrace Basin, Turkey—an interpretation. AAPG Bulletin 75 (2), 241–257.

Perinçek, D., Nurdan Ataş, N., Şeyma Karatut, Ş., Esra Erensoy, E. 2015a. Geological factors controlling potential of lignite beds within the Danişmen Formation in the Thrace Basin. Bulletin of the Mineral Research and Exploration 150, 77-108.

Perinçek, D., Nurdan Ataş, N., Şeyma Karatut, Ş., Esra Erensoy, E. 2015b. Danişmen Formasyonu Stratigrafsi ve Birim İçindeki Linyit Düzeylerinin Havzadaki Dağılımı, Trakya Havzası, Türkiye. Türkiye Jeoloji Bülteni 58(1), 19-62.

Petiau, G. and Dupis, A. 1980. Noise, temperature coefficient, and long time stability of electrodes for telluric observations. Geophysical Prospecting 28, 792-804.

Sakinç, M., Yaltirak, C., Oktay, F.Y. 1999. Paleogeographical evolution of the Thrace Neogene Basin and the Tethys-Paratethyan relations at northwestern Turkey (Thrace). Paleogeographyi Paleoclimatology, Paleoecology 153**,** 17-40.

Siyako, M. 2006. Tertiary rock units of the Thrace Basin (in Turkish). In Lithostratigraphic units of the Thrace region (pp. 55–83). Maden Tetkik ve Arama Genel Müdürlüğü.

Siyako, M., Huvaz, O. 2007. Eocene stratigraphic evolution of the Thrace Basin, Turkey. Sedimentary Geology 198(1–2), 75–91.

Swift, C.M.A. 1967. Magnetotelluric investigation of an electrical conductivity anomaly in the southwestern United States. Ph.D. thesis, Massachusetts Institute of Technology, Cambridge, MA.

Şengör, A.M.C., Yilmaz, Y. 1981. Tethyan evolution of Turkey: A plate tectonic approach. Tectonophysics 75, 181-241.

Turgut, S., Siyako, M., Dilki, A. 1983. The geology and petroleum prospects of the Thrace Basin. Bulletin of the Geological Congress of Turkey 4**,** 35-46.

Turgut, S., Türkaslan, M., Perinçek, D. 1991. Evolution of the Thrace sedimentary basin and its hydrocarbon prospectivity. in A.M. Spencer (Ed.), Generation, accumulation and production of Europe's hydrocarbons. Spec. Publ. Eur. Assoc. Pet. Geosci. 1, 415-437.

Tüysüz, O., Barka, A. Yiğitbaş, E. 1998. Geology of the Saros Graben and its implications for the evolution of the North Anatolian fault in the Ganos-Saros region, Northwestern Turkey. Tectonophysics 293, 105-126.

Vozoff, K. 1972. The magnetotelluric method in the exploration of sedimentary basins: Geophysics 37, 98-141.

Wannamaker, P.E. 1983. Resistivity structure of the Northern Basin and Range, in the role of heat in development of energy and mineral resources in the Northern Basin and Range Province: G. P. Eaton (Ed.), Geoth. Res.Coun. Spec. 13, 345-362.

Wight, D. E., Bostick, F. X. 1980. Cascade decimation: A technique for real time estimation of power spectra. Proceedings IEEE International Conference Accoustic, Speech Signal Processing, Denver, Colorado, April, 9-11, 626-629.

Yilmaz, Y., Tüysüz, O., Yiğitbaş, E., Genç, Ş.C., Şengör, A.M.C. 1997. Geology and tectonic evolution of the Pontides in A. G. Robinson (Ed.) Regional and petroleum geology of the Black Sea and surrounding region: American Association of Petroleum Geologists Memoir, 68, 183-226.